Chiral Separation, X-ray Structure, and Biological Evaluation of a Potent and Reversible Dual Binding Site AChE Inhibitor

Marco Catto, Leonardo Pisani, Eugenio de La Mora, Benny Danilo Belviso, Giuseppe Felice Mangiatordi, Andrea Pinto, Annalisa De Palma, Nunzio Denora, Rocco Caliandro, Jacques-Philippe Colletier, et al.

Chiral Separation, X-ray Structure and Biological Evaluation of a Potent and Reversible Dual Binding Site AChE Inhibitor

Marco Catto[1,*], Leonardo Pisani[1], Eugenio de la Mora[2], Benny Danilo Belviso[3], Giuseppe Felice Mangiatordi[3], Andrea Pinto[4], Annalisa De Palma[5], Nunzio Denora[1], Rocco Caliandro[3], Jacques-Philippe Colletier[2], Israel Silman[6], Orazio Nicolotti[1], Cosimo Damiano Altomare[1]

[1] Department of Pharmacy-Drug Sciences, University of Bari Aldo Moro, Via E. Orabona 4, 70125, Bari, Italy

[2] Univ. Grenoble Alpes, CEA, CNRS, Institute of Structural Biology, F-38044 Grenoble, France.

[3] Institute of Crystallography, National Research Council (CNR), Via G. Amendola 122/O, 70126 Bari, Italy

[4] Department of Food, Environmental and Nutritional Sciences (DeFENS), University of Milan, Via Celoria 2, 20133 Milano (Italy).

[5] Department of Biosciences, Biotechnologies and Biopharmaceutics, University of Bari Aldo Moro, Via E. Orabona 4, 70125, Bari, Italy

[6] Department of Neurobiology, Weizmann Institute of Science, 7610001 Rehovot, Israel.

* Corresponding author; email: marco.catto@uniba.it

ORCID: 0000-0002-8411-304X

Abstract

Acetylcholinesterase (AChE) inhibitors (AChEIs) still remain the leading therapeutic options for the symptomatic treatment of cognitive deficits associated with mild-to-moderate Alzheimer's disease. The search for new AChEIs benefits from well-established knowledge of the molecular interactions of selective AChEIs, such as donepezil and related dual binding site inhibitors. Starting from a

previously disclosed coumarin-based inhibitor (±)-*cis*-**1**, active as racemate in the nanomolar range towards AChE, we proceeded on a double track by: i) achieving chiral resolution of the enantiomers of **1** by HPLC; ii) preparing two close achiral analogues of **1**, *i.e.*, compounds **4** and **6**. An eudismic ratio as high as 20 was observed for the (–) enantiomer of *cis*-**1**. The X-ray crystal structure of the complex between the (−)-*cis*-**1** eutomer (coded as **MC1420**) and *T. californica* AChE was determined at 2.8 Å, and docking calculation results suggested that the eutomer in (1*R*,3*S*) absolute configuration should be energetically more favored in binding the enzyme than the eutomer in (1*S*,3*R*) configuration. The achiral analogues **4** and **6** were less effective in inhibiting AChE compared to (±)-*cis*-**1**, but interestingly butylamide **4** emerged as a potent inhibitor of butyrylcholinesterase (BChE).

Keywords

Dual binding site acetylcholinesterase inhibitors; Alzheimer's disease; coumarin derivatives; X-ray diffraction; molecular docking; chiral separation.

1. Introduction

The increased life expectancy in developed countries represents an unprecedented challenge for health systems and caregivers, due to the widening incidence of age-related pathologies. Among these, neurodegenerative diseases (NDs), most notably, Alzheimer's disease (AD), are considered as a true emergency, because of their increasing incidence and accompanying social and economic costs.[1] AD is a progressive and fatal neurological disease, involving degeneration of brain areas of the frontal cortex and basal forebrain nuclei, which evolves from memory disorders in its early stages, through progressive behavioral alterations that culminate in a total inability in the later stages of the disease.

Despite decades of intensive research, no disease-modifying therapy is yet available, and therapeutic approaches include solely symptomatic treatments based on acetylcholinesterase (AChE) inhibitors (AChEIs) and memantine, an *N*-methyl-D-aspartate (NMDA) receptor antagonist. AChE (EC 3.1.1.7)

is the enzyme principally responsible for the termination of nerve impulse transmission at cholinergic synapses, by rapid hydrolysis of the neurotransmitter acetylcholine (ACh). Cholinergic innervation abounds in regions most affected by neurodegeneration in AD, *e.g.*, the hypothalamus and entorhinal neo-cortex, and accordingly selective inhibition of AChE may help slowing the progress of cognitive alteration in the early stages of the disease. Furthermore, it is commonly accepted that impairment of cholinergic innervation from the nucleus basalis and septal diagonal band to the cerebral cortex and hippocampus are involved in producing the cognitive changes.[2] While effectiveness decreases along with the progression of AD, this approach is to date the only option for alleviating symptoms.[3] In the central nervous system (CNS), AChE activity is complemented by that of butyrylcholinesterase (BChE), a related enzyme characterized by a larger active site, and thus capable of accommodating larger substrates. BChE is present in the serum and in the CNS, where its concentration increases with the progression of AD, colocalising with neuritic plaques.[4] These observations have supported the hypothesis that BChE might serve as a target for the symptomatic treatment of late-stage AD.[5,6] The observation that cymserine analogues, selectively targeting BChE, can partially restore AChE brain levels and cognitive functions in aged rats[7] provides support for this hypothesis.

3D structures of AChE from several species, *e.g.*, *Torpedo*, electric eel, mouse, and human,[8] in the presence or absence of inhibitors, have been solved by X-ray crystallography, demonstrating the existence of two binding sites at the top and bottom of the active-site gorge, termed the peripheral anionic site (PAS), and the catalytic anionic site (CAS), respectively.[9] Among AChEIs, donepezil (Figure 1) is considered as a reference drug because of its potency and high therapeutic index. Its peculiar inhibitory mechanism involves a dual binding site (DBS) reversible interaction with both the CAS and the PAS of the enzyme, thus resulting in mixed, i.e. neither completely competitive nor noncompetitive, inhibition kinetics.[10,11]

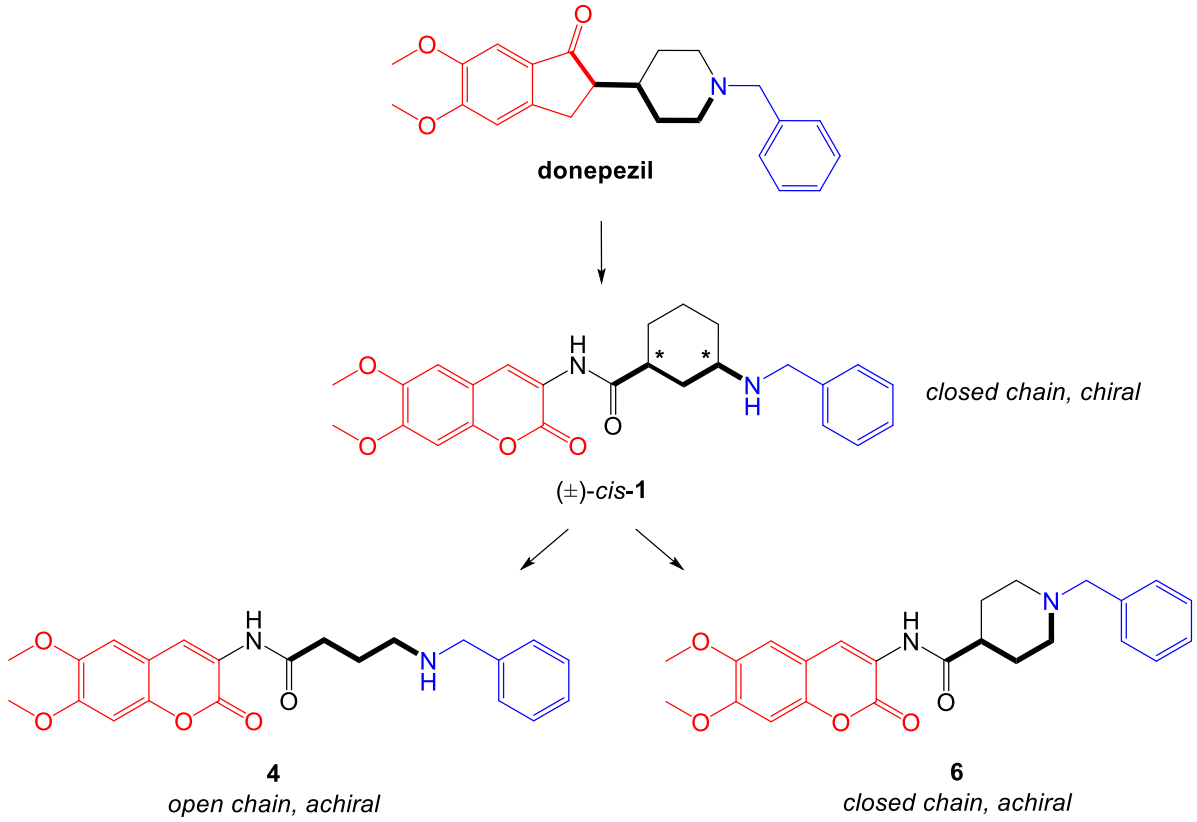

Figure 1. Ligand-based design of dual binding site inhibitors of AChE.

Many DBS inhibitors of AChE have been described in the literature,[12] often displaying potent, reversible, and selective inhibition.[13] Many of them exhibit the archetypal structural features of donepezil, *i.e.*, a protonatable *N*-benzylamine moiety able to interact with the aromatic amino acids of the CAS, and a planar, aromatic, lipophilic terminal portion making hydrophobic interactions (mainly π-π stacking) within the PAS. These structural features were indeed displayed by the coumarin-based racemic compound (±)-*cis*-**1** (Figure 1), which has been studied by some of the authors of the current study.[14] To assess the stereochemical contribution to AChE inhibition of the *cis*-3-amino-1-ciclohexanecarboxylic acid used as the spacer in (±)-*cis*-**1**, we performed its chiral separation by HPLC, and tested the two enantiomers. In parallel, we undertook the design of two new achiral analogues **4** and **6**, also shown in Figure 1. Compound **4** includes a 3-atom linear open chain, and **6** encloses a piperidine ring, both joined to the donepezil-like *N*-benzyl moiety. By employing docking-assisted crystallographic studies, we determined the crystal structure of compound (–)-*cis*-**1**

(coded as **MC1420**), established as the eutomer after chiral separation, complexed with *Torpedo californica* AChE (*Tc*AChE). Scheme 1 shows the synthetic and experimental procedure for obtaining **4**, **6**, and the two chiral forms of (±)-*cis*-**1**. Permeability and cytotoxicity of the coumarin derivative (±)-*cis*-**1** were also evaluated *in vitro* as an early assessment of its potential as an AChE inhibitor for alleviating symptoms in AD-associated cognitive impairments.

Scheme 1[a]

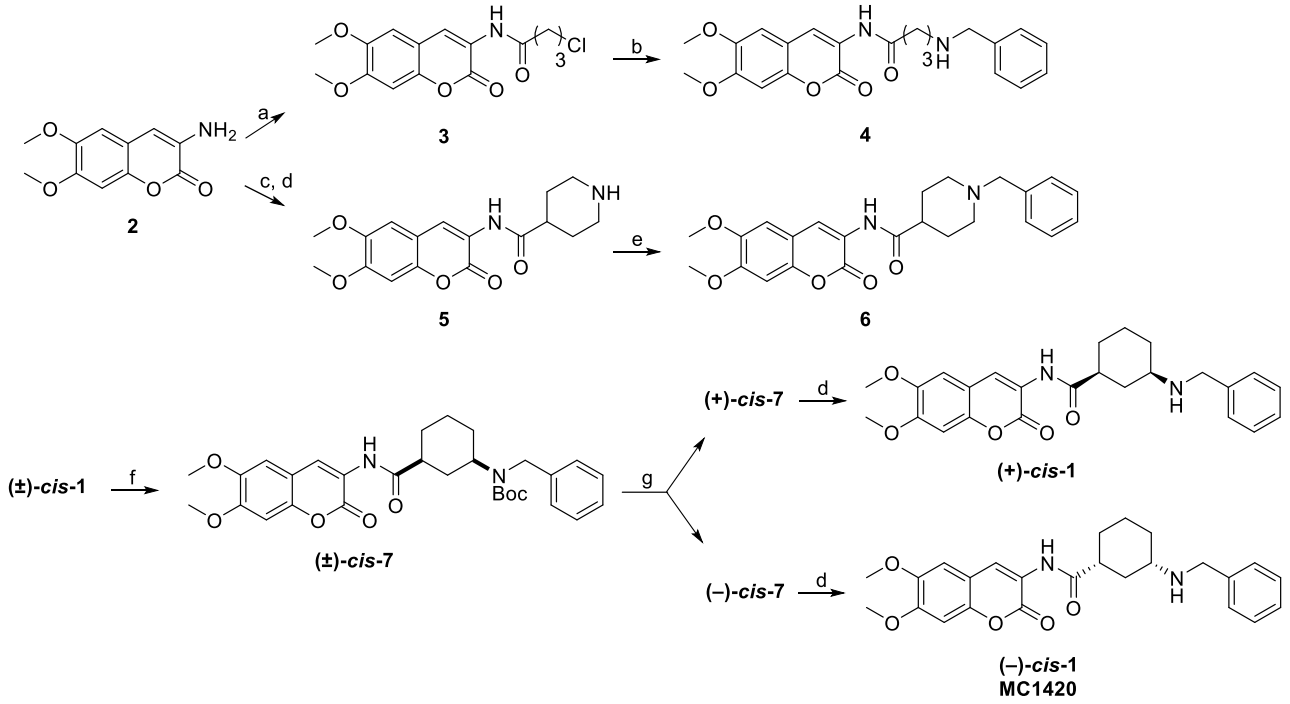

([a]) Reagents and conditions: (a), 4-chlorobutyryl chloride, THF, triethylamine, rt; (b), benzylamine, KI, acetone, rt; (c), *N*-Boc protected isonipecotic acid, HOBt, DIC, CH_2Cl_2, rt; (d), TFA, CH_2Cl_2, 0 °C. (e), benzyl bromide, K_2CO_3, acetone, rt; (f) Boc_2O, THF, rt; (g) semi-preparative chiral HPLC.

Previous data on coumarin-donepezil hybrid (±)-*cis*-**1** highlighted a good inhibitory potency on electric eel AChE (*ee*AChE) with very high selectivity over BChE.[14] In order to obtain data comparable with published works in which the inhibition of human isoforms (*h*AChE, *h*BChE) were studied, we first investigated the inhibition of *h*AChE and *h*BChE by (±)-*cis*-**1**. The IC_{50} value for (±)-*cis*-**1** against *h*AChE in Table 1 (36.5 nM) is in fair agreement with that previously determined

for *ee*AChE (7.6 nM).[14] The *h*AChE kinetic inhibition constant (K_i) of (±)-*cis*-**1** was four-fold higher than that measured for donepezil (46.6 *vs*. 12.7 nM, Table 1). The kinetic profile correlated well with a mixed-mode inhibition, typical for putative DBS inhibitors.

Table 1. Inhibition data of title compounds.[a]

Entry	IC_{50} (nM)		K_i *h*AChE (nM)
	***h*AChE**	***h*BChE**	
(±)-*cis*-**1**	36.5 ± 5.4	6250 ± 906	46.6 ± 3.6 *(mixed)*
(+)-*cis*-**1**	380 ± 45	2330 ± 219	93.4 ± 3.2 *(mixed)*
(−)-*cis*-**1** (**MC1420**)	19.2 ± 3.0	14100 ± 205	19.1 ± 1.4 *(mixed)*
4	748 ± 24	181 ± 7	n.d.
6	223 ± 5	*21 ± 2%*[b]	n.d.
Donepezil	16.1 ± 2.7	2900 ± 500	12.7 ± 1.0 *(mixed)*

([a]) Values are mean ± SEM of three independent experiments; n.d.: not determined. ([b]) % inhibition at 10 μM.

A preliminary assessment of safety profile was obtained from a MTT-based cellular test[15] of (±)-*cis*-**1**, which was incubated with HepG2 human liver cancer cells in the 20-100 μM concentration range (Figure 2). Cell viability after 2 h was always 80-90% even at the higher concentrations, thus revealing a low intrinsic cytotoxicity.

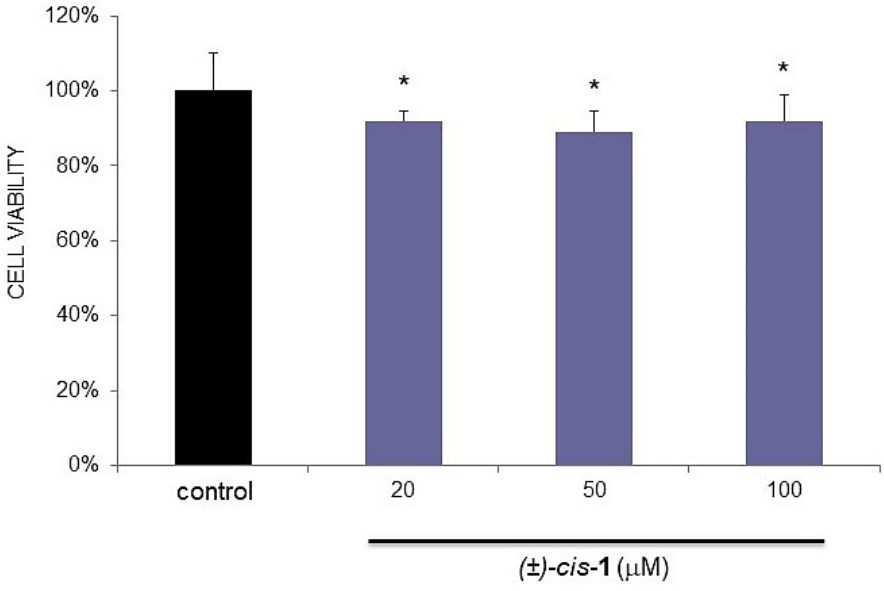

Figure 2. HepG2 cells viability, measured by the MTT assay, in the absence (black bar) and presence (grey bars) of (±)-*cis*-**1**. The percentage of MTT reduction observed is relative to control cells (DMEM). Values are expressed as mean ± SEM from six replicates, being significantly different from the control (untreated cells) as estimated by the Student's *t* test (**p* < 0.01).

The potential of (±)-*cis*-**1** as a hit compound for pharmacological profiling was further explored by assessing its permeability in a well-validated cell membrane model, which utilizes the MDCK-MDR1 cell line expressing the efflux system P-gp. This cell line is widely considered to reliably mimic blood-brain barrier permeability, accounting for both transcellular and paracellular pathways.[16] The MTT assay of cell viability, performed after 24 and 72 h of coincubation with 100 μM (±)-*cis*-**1**, showed lower cell survival compared with the control HepG2 samples, with cell viability dropping to 60% and 37%, respectively (Supporting Information, Table S1). However, the IC_{50} at this last time point was 30 μM, a value three orders of magnitude higher than the IC_{50} measured for AChE. Following a previously reported approach,[17] the apparent permeabilities P_{app} were measured both from the apical to basolateral (P_{app} AP) and from the basolateral to apical (P_{app} BL) compartments. Diazepam and FD-4 were used as markers of transcellular and paracellular pathways, respectively. The permeability values shown in Table 2 are comparable to those of reference compounds, while the efflux ratio lower than 2 that was found indicates that the compound is not a substrate for P-gp.

Table 2. Permeability assay data.[a]

Entry	P_{app} AP ($\times 10^{-5}$ cm/s)	P_{app} BL ($\times 10^{-5}$ cm/s)	ER (P_{app} BL/ P_{app} AP)
(±)-*cis*-**1**	3.7 ±1.2	0.84 ± 0.20	0.22
Diazepam	2.0 ± 0.2	1.4 ± 0.2	0.70
FD-4	0.69 ± 0.10	0.65 ± 0.12	0.93

([a]) Values are mean ± SEM of three independent experiments.

With this information in hand, we proceeded with the enantiomeric separation of (±)-*cis*-**1**. Due to the presence of a secondary *N*-benzylamine group, we performed a preliminary *N*-Boc protection, leading to the lipophilic derivative **7** (Scheme 1). Resolution of racemate (±)-*cis*-**7** into the single enantiomers was achieved by semi-preparative chiral HPLC (Figure 3), using a Kromasil 5-AmyCoat chiral stationary phase with isopropanol/*n*-hexane 1:1 v/v as the mobile phase, followed by Boc deprotection.

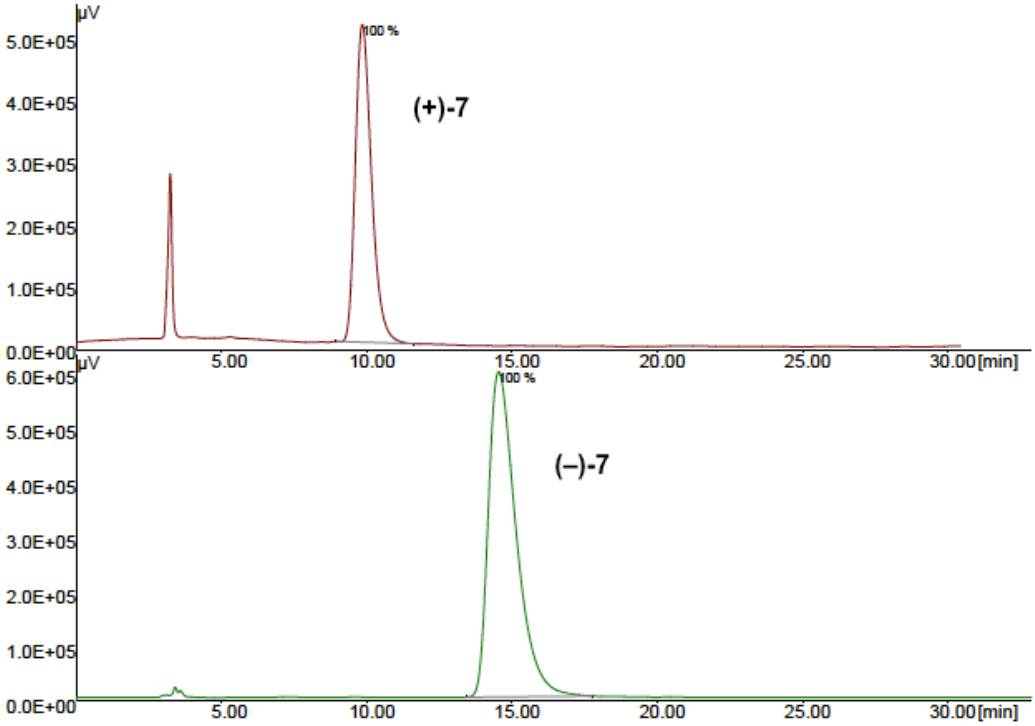

Figure 3. Chromatograms of enantiopure samples obtained by chiral resolution of (±)-*cis*-**7**.

Inhibition data reported in Table 1 show a eudismic ratio of *ca.* 20 for the (–) enantiomer (coded as **MC1420**), with IC_{50} for *h*AChE very close to that of donepezil. Interestingly, an opposite eudismic ratio was found for *h*BChE inhibition, leading to high (730-fold) AChE/BChE selectivity of **MC1420**. The K_i for **MC1420** was 19.1 nM, close to the value of 12.7 nM found for donepezil, and the kinetic data fitted a Michaelis-Menten model of a mixed-type inhibition, with very low variance (residuals < ± 1%; $r^2 = 0.996$; Figure 4).

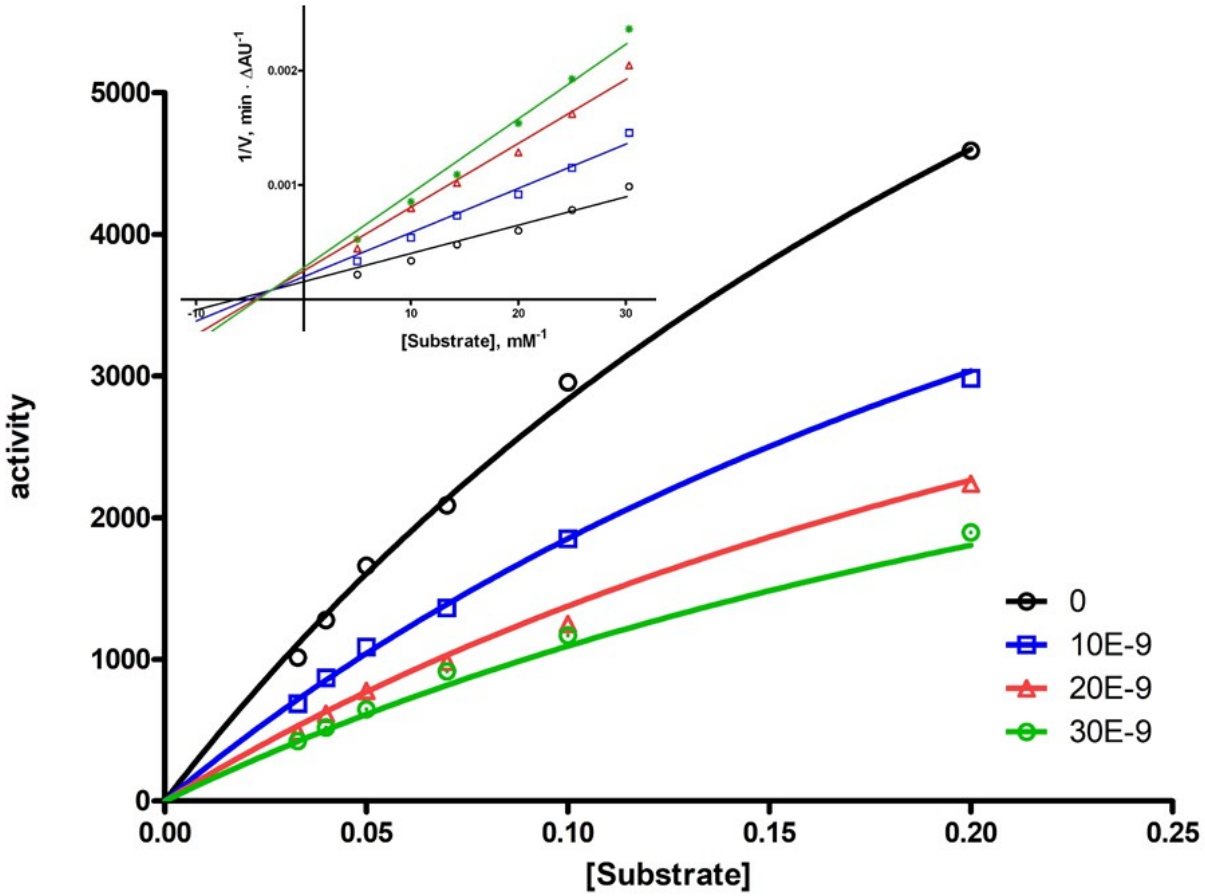

Figure 4. Michaelis-Menten plot for inhibition of *h*AChE by **MC1420** at various inhibitor concentrations. The inset displays the corresponding Lineweaver-Burk plot.

As shown in Table 1, the newly synthesized derivatives **4** and **6** (Scheme 1) were unable to reproduce the good inhibitory capacity of racemate **1**. As far as compound **4** is concerned, we replaced the conformationally constrained cyclohexyl spacer with a linear open chain. This structural variation turned out to be detrimental, resulting in a 20-fold activity drop in inhibition of *h*AChE. The second structural variation was designed to keep the six-atom ring spacer, while incorporating the basic nitrogen into an *N*-benzylpiperidine fragment, which is a typical pharmacophore motif of donepezil and related structures. The isonipecotamide derivative **6** showed a 6-fold drop in *h*AChE inhibition compared to *rac*-**1** while retaining fair AChE inhibition and very high AChE/BChE selectivity. It is noteworthy that the butylamide **4** showed strong inhibition of *h*BChE, thus resulting as a good and

fairly selective inhibitor of this isozyme. The decrease in activity returned by these achiral analogues, irrespective of the limited variation in distance between the basic nitrogen and the coumarin moiety, interacting at the CAS and PAS, respectively, prompted us to elucidate the interactions of **MC1420** with its target protein at the molecular level.

We thus determined the crystal structure of the complex of eutomer **MC1420** with *Tc*AChE. **MC1420** was soaked into trigonal crystals of *Tc*AChE, obtained as described earlier,[18] and the structure of the *Tc*AChE/**MC1420** complex (PDB ID: 6TT0) was solved at 2.8 Å resolution from data collected at 100 K at a synchrotron beamline, following cryoprotection and flash-cooling of crystals. At this stage, the absolute configuration of **MC1420** at the 1,3-*cis*-cyclohexyl ring spacer, namely, either (1*R*,3*S*) or (1*S*,3*R*), was unknown. Therefore, the structural refinement was performed assuming both the configurations of the spacer. In both cases, it was observed that the ligand molecule binds to the CAS through its *N*-benzyl moiety, with the coumarin group anchored at the PAS (Figure 5). This binding mode is driven mainly by two π-π stacking interactions, that of the aromatic ring of the *N*-benzyl group of the ligand with the indole of Trp84 (Trp86 in *h*AChE) in the CAS, and of the coumarin ring with the indole moiety of Trp279 (Trp286 in *h*AChE) in the PAS. Regardless of the ligand's absolute configuration, the rings involved in these stacking interactions are almost parallel (interplanar angle < 15°) and display the typical parallel-displaced geometry. Interestingly, the interplanar distance between the coumarin group and Trp279 is about 0.5 Å shorter than that between Trp84 in the CAS and the *N*-benzyl group of the ligand.

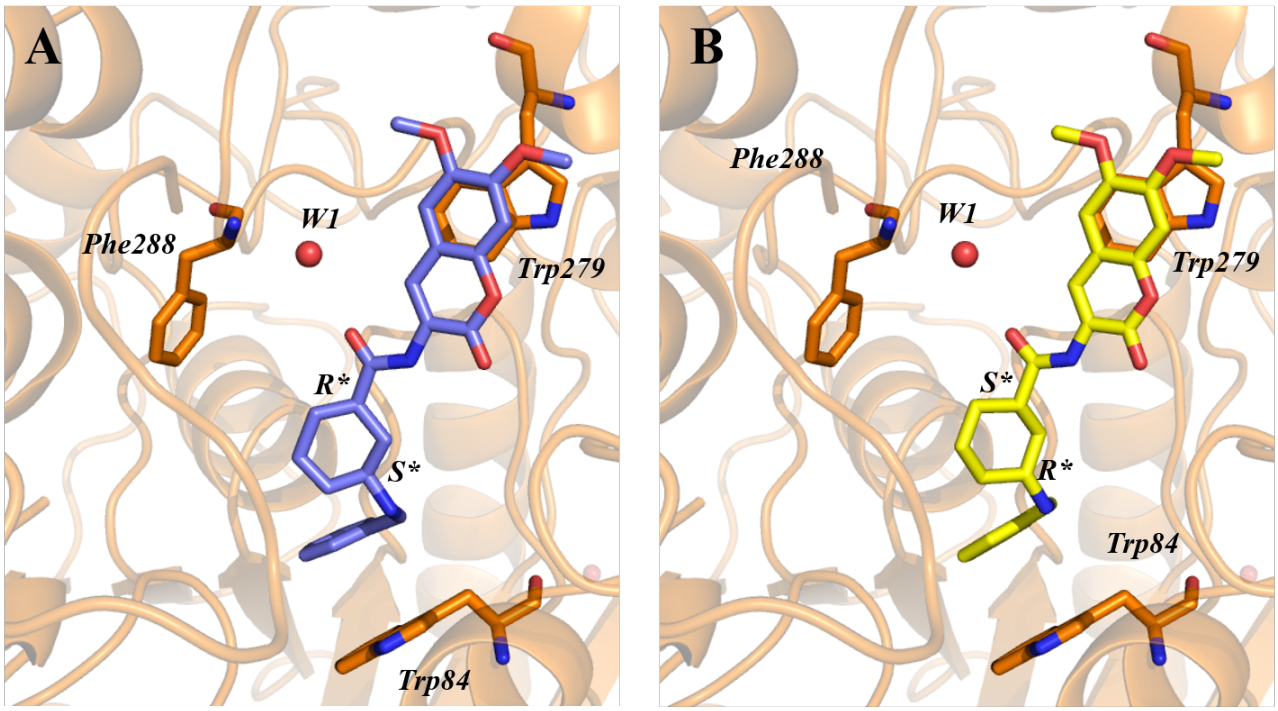

Figure 5. X-ray structure of the **MC1420**/*Tc*AChE complex (PDB ID: 6TT0). Data refined for the 1*R*,3*S*-*cis*- (A) and 1*S*,3*R*-*cis*- (B) configurations. The ligands and relevant amino acid residues are rendered as sticks, the water molecule W1 responsible for a water-mediated interaction with Phe288 is shown as a red sphere, while protein is represented as cartoon.

The experimental electron density map revealed the presence of a water molecule (W1 in Figure 5) at 2.8 Å from the oxygen atom of the amide group of **MC1420**, and 2.7 Å from the nitrogen atom of the Phe288 backbone, distances both compatible with H-bond interactions. This water-mediated interaction, along with the two stacking interactions described above, comprise the whole set of significant protein-ligand interactions. The oxygen of W1 has a thermal factor (59.4 $Å^2$) that agrees very well with the average B-factor of atoms within 5 Å of W1 (60 $Å^2$). Importantly, the B-factor is obtained by using W1 at full crystallographic occupancy, suggesting that this water molecule and related water-mediated interactions are present in each unit of the crystal. By performing hydration analysis of the ligand by wet script, two water molecules were identified close to the one observed experimentally (Figure S1 in Supporting Information). Interestingly, W1 corresponds to a conserved water as identified by Koellner *et al.*,[19] and it therefore preexists at this position before binding of the

compound. The structure offers an illustration that this structural water is indeed fully part of the gorge, where it helps to accommodate (and determine the binding affinity) of **MC1420** in the gorge. Despite the ligand being clearly visible in the experimental Fo-Fc electron density map, the absolute configuration of the (–)-*cis*-**1** ligand used in the crystal preparation could not be unambiguously determined at the achieved resolution. We additionally performed molecular docking simulations, followed by binding free energy calculations for both configurations. Given the importance of W1 for ligand binding, this water molecule was included in the docking calculations performed.

(1*R*,3*S*)-*cis*-**1** returned not only a better docking score (-13.56 kcal/mol) and a better binding free energy (-99.28 kcal/mol) than (1*S*,3*R*)-*cis*-**1** (-11.74 kcal/mol and -81.00 kcal/mol respectively), but also a more plausible pose, as shown by comparing Figures 5 and 6. We may postulate that this difference can be accounted for by an additional interaction with the PAS, established only by the (1*R*,3*S*) configuration (Figure 6). The *S* configuration of the carbon atom at position 3 of the cyclohexane should more likely permit an orientation of the charged amine adjacent to the benzyl ring, prone to form a salt bridge with Asp72. Taken together, these data suggest that **MC1420** in the (1*R*,3*S*)-*cis* configuration should be more favored in binding compared to (1*S*,3*R*)-*cis* configuration. Noteworthy, the eutomer in both configurations should form a water-bridged H-bond with Phe288 in the acyl pocket.

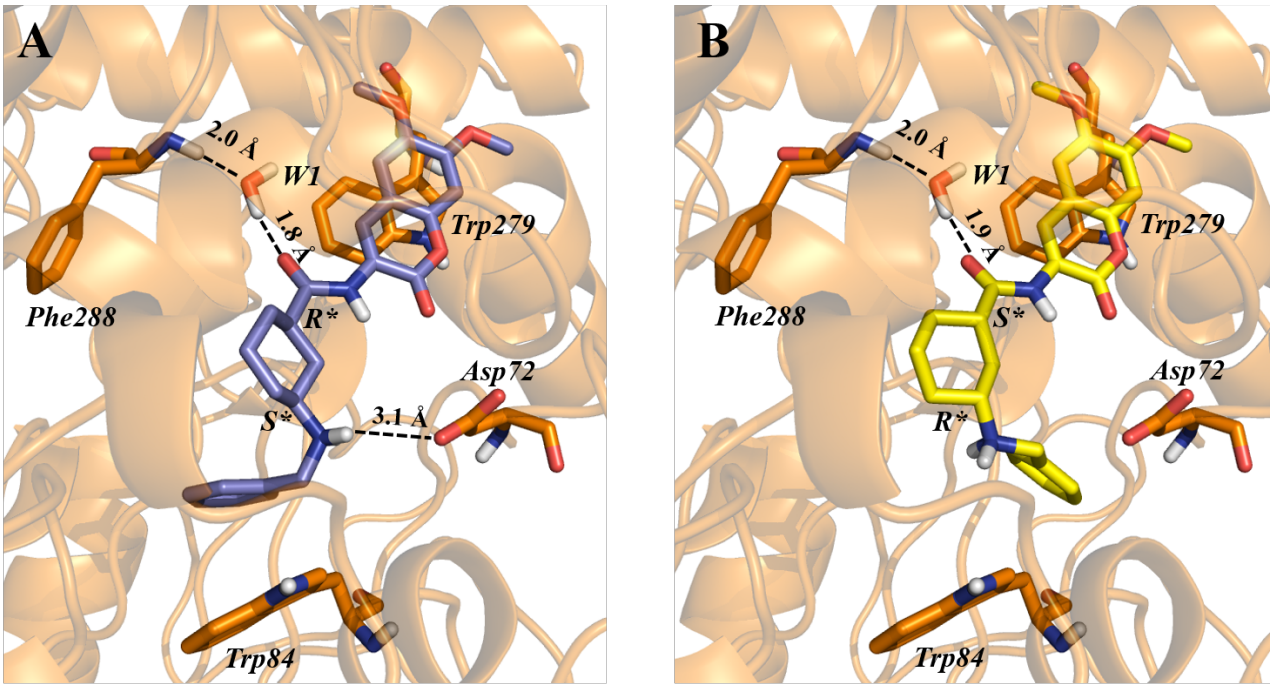

Figure 6. Top-scored docking poses for the (1R,3S)-*cis*- (A) and (1S,3R)-*cis*- (B) configurational isomers of **1** within the binding site of *Tc*AChE. The ligand itself, relevant amino acid residues, and the water molecule W1 responsible for water-mediated interaction with Phe288, are all rendered as sticks, while protein is represented as cartoon. H-bonds are depicted by dotted lines.

In agreement with the experimental findings, even the best solutions for achiral compounds **4** and **6** returned poorer docking scores (-11.44 kcal/mol and -12.34 kcal/mol, respectively) as well as poorer binding free energies (-79.49 kcal/mol and -78.70 kcal/mol, respectively) relative to (1*R*,3*S*)-*cis*-**1**. The obtained top-scored docking poses are reported in the Supporting Information (Figure S2).

In conclusion, our efforts to design selective and reversible AChE/BChE inhibitors led us to the synthesis of the AChE-selective hit compound (±)-*cis*-**1** (Figure 1),[14] which showed *in vitro* good safety and capacity to cross the BBB as assessed by HepG2 and MDCKII-MDR cell-based assays, respectively. After chiral resolution, the (–)-*cis*-**1** enantiomer **MC1420** resulted the eutomer in *h*AChE inhibition, thus justifying the use of X-ray crystallography to resolve its binding mode in complex with *Tc*AChE. The structure confirmed the dual binding mode of interaction predicted for

MC1420, whereas docking calculations suggested that **MC1420** should more favorably bind the enzyme in (1*R*,3*S*) absolute configuration than in (1*S*,3*R*).

Furthermore, in an attempt to overcome stereoisomeric limitations in a possible pharmacological evaluation, two achiral congeners of (±)-*cis*-**1**, i.e. **4** and **6**, were synthesized and tested. These compounds did not replicate the strong inhibitory potency of **1**. However, the butylamide **4** displayed good inhibition of BChE (IC_{50} = 181 nM) and the piperidine derivative **6** a high (about two orders of magnitude) AChE/BChE selectivity, suggesting that both of them could deserve further consideration.

Materials and methods

*Structure determination of the **MC1420**/TcAChE complex*

After chiral separation of (±)-*cis*-**1** racemate, the (–)-*cis*-**1** enantiomer **MC1420** was soaked for 2 h at 1 mM concentration in hanging drops containing trigonal crystals of *Tc*AChE, obtained as described previously.[18] Crystals were then flash-cooled, *in situ,* at 100 K under the gaseous nitrogen stream of a cryo-cooler (Oxford Cryosystems, Oxford, United Kingdom). Data collection was carried out on beamline ID29, at the European Synchrotron Facility (ESRF) at a wavelength of 1.074 Å. Initial phases were determined by rigid-body refinement using as a model the native *Tc*AChE structure (PDB ID 2VT7). The Fo-Fc difference map showed continuous positive electron density at $\sigma > 3.5$ within the active site gorge of the enzyme (CAS and PAS). Both enantiomers compatible with **MC1420** in *cis* conformation (1R,3S and 1S,3R of the cyclohexane ring) were tested in the refinement procedure. The restrain description file required for the refinement procedure was generated by using the PRODRG server[20] and modified to ensure planarity of the coumarin and amide groups. Molecular geometry was optimized by eLBOW,[21] under the crystallographic suite PHENIX.[22] The ligand was fitted into the positive *Fo-Fc* Fourier difference map by using COOT.[23] Water molecules were then added to the protein-ligand complex and the resulting crystal structure was refined using *phenix.refine*,[24] included in the Phenix crystallographic software suite.[22] The structural model was validated using the Phenix implementation of MolProbity.[25]

Docking simulations

Both enantiomers of (±)-*cis*-**1** were docked into the refined X-ray structure of the complex 6TT0. The protein structure was prepared using Protein Preparation Wizard[26] for adding missing hydrogen

atoms, reconstructing incomplete side chains and loops, and assigning ambiguous protonation states. The ligand was prepared using LigPrep[26] in order to properly generate all the possible tautomers and ionization states at a pH value of 7.0 ± 2.0. The files thus obtained were used for docking simulations performed by Grid-based ligand docking with energetics (GLIDE).[26,27] During the docking process, the protein was held fixed, whereas full conformational flexibility was allowed for the ligand. The default Force Field OPLS_2005,[28] and all the default settings of the extra precision (XP) protocol were used. A cubic grid was used that was centered on the refined structure of the cognate ligand, having an edge of 10 Å for the inner box and 30 Å for the outer box. Finally, a water molecule (referred to as W1) was kept in the binding site during docking simulations. Indeed, W1 arises from experimental electron density indicating a water-mediated H-bond involving the carbonyl group of the ligand and the backbone of Phe288.

MM-GBSA calculations

The binding free energies (ΔG) between protein and ligands were computed by applying the Molecular Mechanics/Generalized Born Surface Area on the obtained top-scored docking poses.[29] More specifically, Prime[30] was the software used, and the following Equation 1 was applied:

$$\Delta E_{bind} = \Delta E_{MM} + \Delta G_{solv} + \Delta G_{SA} \qquad (1)$$

where ΔE_{MM}, ΔG_{solv} and ΔG_{SA} represent the difference between the contribution made by the ligand-protein complex and the sum of those made by the ligand and the protein taken alone, in terms of minimized energy, solvation energy and surface area energy, respectively. Flexibility was allowed for all residues having at least one atom within a distance of 3 Å from the ligand.

Associated Content

Supporting Information

Syntheses of compounds **4-6**, procedures for chiral separation of (±)-*cis*-**1**, cell viability assays (Table S1), hydration calculations for **MC1420** (Figure S1), docking of compounds **4** and **6** (Figure S2), and crystallographic data (Table S2) are reported as Supporting Information. This material is available free of charge via the internet at http://pubs.acs.org.

References

1. Alzheimer's Association. 2019 Alzheimer's disease facts and figures. *Alzheimers Dement.* **2019**, *15*, 321-387.

2. Mufson, E. J.; Counts, S. E.; Perez, S. E.; Ginsberg, S. D. Cholinergic System during the Progression of Alzheimer's Disease: Therapeutic Implications. *Expert Rev. Neurother*. **2008**, *8*, 1703-1718.

3. Graham, W. V.; Bonito-Oliva, A.; Sakmar, T.P. Update on Alzheimer's Disease Therapy and Prevention Strategies. *Annu. Rev. Med.* **2017**, *68*, 413-430.

4. Macdonald, I. R.; Maxwell, S. P.; Reid, G. A.; Cash, M. K.; DeBay, D. R.; Darvesh, S. Quantification of Butyrylcholinesterase Activity as a Sensitive and Specific Biomarker of Alzheimer's Disease. *J. Alzheimers Dis*. **2017**, *58*, 491-505.

5. Greig, N. H.; Utsuki, T.; Yu, Q.-S.; Zhu, X.; Holloway, H. W.; Perry, T. A.; Lee, B.; Ingram, D. H.; Lahiri, D. K. A New Therapeutic Target in AD Treatment: Attention to Butyrylcholinesterase. *Curr. Med. Res. Opin.* **2001**, *17*, 159-165.

6. de Candia, M.; Zaetta, G.; Denora, N.; Tricarico, D.; Majellaro, M.; Cellamare, S.; Altomare, C. D. New Azepino[4,3-b]indole Derivatives as Nanomolar Selective Inhibitors of Human Butyrylcholinesterase Showing Protective Effects against NMDA-induced Neurotoxicity. *Eur. J. Med. Chem*. **2017**, *125*, 288-298.

7. Greig, N. H.; Utsuki, T.; Ingram, D. K.; Wang, Y.; Pepeu, G.; Scali, C.; Yu, Q. S.; Mamczarz, J.; Holloway, H. W.; Giordano, T.; Chen, D.; Furukawa, K.; Sambamurti, K.; Brossi, A.; Lahiri, D. K. Selective Butyrylcholinesterase Inhibition Elevates Brain Acetylcholine, Augments Learning and Lowers Alzheimer Beta-amyloid Peptide in Rodent. *Proc. Natl. Acad. Sci. U S A* **2005**, *102*, 17213-17218.

8. Cheung, J.; Rudolph, M. J.; Burshteyn, F.; Cassidy, M. S.; Gary, E.N.; Love, J.; Franklin, M. C.; Height, J. J. Structures of Human Acetylcholinesterase in Complex with Pharmacologically Important Ligands. *J. Med. Chem.* **2012**, *55*, 10282-10286.

9. Greenblatt, H. M.; Dvir, H.; Silman, I.; Sussman, J. L. Acetylcholinesterase: a Multifaceted Target for Structure-based Drug Design of Anticholinesterase Agents for the Treatment of Alzheimer's Disease. *J. Mol. Neurosci.* **2003**, *20*, 369-383.

10. Nochi, S.; Asakawa, N.; Sato, T. Kinetic Study on the Inhibition of Acetylcholinesterase by 1-Benzyl-4-((5,6-dimethoxy-1-indanon)-2-yl)methylpiperidine Hydrochloride (E2020). *Biol. Pharm. Bull.* **1995**, *18*, 1145-1147.

11. Kryger, G.; Silman, I.; Sussman, J. L. Structure of Acetylcholinesterase Complexed with E2020 (Aricept): Implications for the Design of New Anti-Alzheimer Drugs. *Structure* **1999**, *7*, 297-307.

12. Wang, Y.; Wang, H.; Chen, H. Z. AChE Inhibition-based Multi-target-directed Ligands, a Novel Pharmacological Approach for the Symptomatic and Disease-modifying Therapy of Alzheimer's Disease. *Curr. Neuropharmacol*. **2016**, *14*, 364-375.

13. Pisani, L.; Catto, M.; De Palma, A.; Farina, R.; Cellamare, S.; Altomare, C. D. Discovery of Potent Dual Binding Site Acetylcholinesterase Inhibitors via Homo- and Heterodimerization of Coumarin-Based Moieties. *ChemMedChem* **2017**, *12*, 1349-1358.

14. Catto, M.; Pisani, L.; Leonetti, F.; Nicolotti, O.; Pesce, P.; Stefanachi, A.; Cellamare, S.; Carotti, A. Design, Synthesis and Biological Evaluation of Coumarin Alkylamines as Potent and Selective Dual Binding Site Inhibitors of Acetylcholinesterase. *Bioorg. Med. Chem.* **2013**, *21*, 146-152.

15. Berridge, M. V.; Tan, A. S. Characterization of the Cellular Reduction of 3-(4,5-Dimethylthiazol-2-yl)-2,5-diphenyltetrazolium Bromide (MTT): Subcellular Localization, Substrate Dependence, and

Involvement of Mitochondrial Electron Transport in MTT Reduction. *Arch. Biochem. Biophys.* **1993**, *303*, 474-482.

16. Franchini, S.; Manasieva, L.I.; Sorbi, C.; Battisti, U. M.; Fossa, P.; Cichero, E.; Denora, N.; Iacobazzi, R. M.; Cilia, A.; Pirona, L.; Ronsisvalle, S.; Aricò, G.; Brasili, L. Synthesis, Biological Evaluation and Molecular Modeling of 1-Oxa-4-thiaspiro- and 1,4-Dithiaspiro[4.5]decane Derivatives as Potent and Selective 5-HT_{1A} Receptor Agonists. *Eur. J. Med. Chem.* **2017**, *125*, 435-452.

17. Pisani, L.; Farina, R.; Soto-Otero, R.; Denora, N.; Mangiatordi, G. F.; Nicolotti, O.; Mendez-Alvarez, E.; Altomare, C. D.; Catto, M.; Carotti, A. Searching for Multitargeting Neurotherapeutics against Alzheimer's: Discovery of Potent AChE−MAO B Inhibitors through the Decoration of 2H-Chromen-2-one Structural Motif. *Molecules* **2016**, *21*, 362.

18. Dighe, S. N.; De la Mora, E.; Chan, S.; Kantham, S.; McColl, G.; Miles, J. A.; Veliyath, S. K.; Sreenivas, S. K.; Nassar, Z. D.; Silman, I.; Sussman, J. L.;Weik, M.; McGeary, R. P.; Parat, M. O.; Brazzolotto, X.; Ross, B. P. Rivastigmine and Metabolite Analogues with Putative Alzheimer's Disease-modifying Properties in a *Caenorhabditis elegans* Model. *Commun. Chem*. **2019**, *2*, 35.

19. Koellner, G.; Kryger, G.; Millard, C. B.; Silman, I.; Sussman, J. L.; Steiner, T. Active-site Gorge and Buried Water Molecules in Crystal Structures of Acetylcholinesterase from Torpedo californica. *J. Mol. Biol.* **2000**, *296*, 713-735.

20. Schüttelkopf, A. W.; van Aalten, D. M. F. PRODRG: A Tool for High-Throughput Crystallography of Protein-Ligand Complexes. *Acta Crystallogr. D Biol. Crystallogr.* **2004**, *60*, 1355-1363.

21. Moriarty, N. W.; Grosse-Kunstleve, R. W.; Adams, P. D. Electronic Ligand Builder and Optimization Workbench (eLBOW): a tool for ligand coordinate and restraint generation. *Acta Crystallogr. D Biol. Crystallogr.* **2009**, *65*, 1074-1080.

22. Adams, P. D.; Afonine, P. V.; Bunkóczi, G.; Chen, V. B.; Davis, I. W.; Echols, N.; Headd, J. J.; Hung, L. W.; Kapral, G. J.; Grosse-Kunstleve, R. W.; McCoy, A. J.; Moriarty, N. W.; Oeffner, R.; Read, R. J.; Richardson, D. C.; Richardson, J. S.; Terwilliger, T. C.; Zwart, P. H. PHENIX: A Comprehensive Python-based System for Macromolecular Structure Solution. *Acta Crystallogr. D Biol. Crystallogr*. **2010**, *66*, 213-221.

23. Emsley, P.; Lohkamp, B.; Scott, W. G.; Cowtan, K. Features and Development of Coot. *Acta Crystallogr. D Biol. Crystallogr*. **2010**, *66*, 486-501.

24. Afonine, P. V.; Grosse-Kunstleve, R. W.; Echols, N.; Headd, J. J.; Moriarty, N. W.; Mustyakimov, M.; Terwilliger, T. C.; Urzhumtsev, A.; Zwart, P. H.; Adams, P. D. Towards Automated Crystallographic Structure Refinement with phenix.refine. *Acta Crystallogr. D Biol. Crystallogr*. **2012**, *68*, 352-367.

25. Chen, V. B.; Arendall, W. B. 3rd; Headd, J. J.; Keedy, D. A.; Immormino, R. M.; Kapral, G. J.; Murray, L. W.; Richardson, J. S.; Richardson, D. C. MolProbity: All-atom Structure Validation for Macromolecular Crystallography. *Acta Crystallogr. D Biol. Crystallogr.* **2010**, *66*, 12-21.

26. Schrödinger Suite 2018-4 Protein Preparation Wizard, Schrödinger, LLC, New York, NY, 2018.

27. Friesner, R. A.; Murphy, R. B.; Repasky, M. P.; Frye, L. L.; Greenwood, J. R.; Halgren, T. A.; Sanschagrin, P. C.; Mainz, D. T. Extra Precision GLIDE: Docking and Scoring Incorporating a Model of Hydrophobic Enclosure for Protein-Ligand Complexes. *J. Med. Chem*. **2006**, *49*, 6177-6196.

28. Robertson, M. J.; Tirado-Rives, J.; Jorgensen, W. L. Improved Peptide and Protein Torsional Energetics with the OPLSAA Force Field. *J. Chem. Theory. Comput*. **2015**, *11*, 3499-3509.

29. Genheden, S.; Ryde, U. The MM/PBSA and MM/GBSA Methods to Estimate Ligand-Binding Affinities. *Expert Opin. Drug Discov*. **2015**, *10*, 449-461.

30. PrimeX, Schrödinger, LLC, New York, NY, 2018.

Table of Contents Graphic (For Table of Contents Use Only)

Chiral Separation, X-ray Structure and Biological Evaluation of a Potent and Reversible Dual Binding Site AChE Inhibitor

Marco Catto*, Leonardo Pisani, Eugenio de la Mora, Benny Danilo Belviso, Giuseppe Felice Mangiatordi, Andrea Pinto, Annalisa De Palma, Nunzio Denora, Rocco Caliandro, Jacques-Philippe Colletier, Israel Silman, Orazio Nicolotti, Cosimo Damiano Altomare

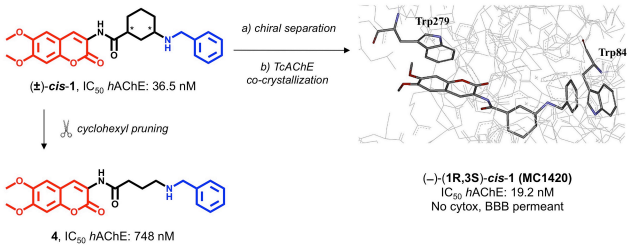

Lay summary

Enantiomerically pure **MC1420**, a brain-permeant, potent dual binding site AChE inhibitor, has been crystallized in complex with *Tc*AChE and its binding mode investigated by comparing X-ray data and docking studies.

Chiral Separation, X-ray Structure and Biological Evaluation of a Potent and Reversible Dual Binding Site AChE Inhibitor

Marco Catto[1,*], Leonardo Pisani[1], Eugenio de la Mora[2], Benny Danilo Belviso[3], Giuseppe Felice Mangiatordi[3], Andrea Pinto[4], Annalisa De Palma[5], Nunzio Denora[1], Rocco Caliandro[3], Jacques-Philippe Colletier[2], Israel Silman[6], Orazio Nicolotti[1], Cosimo Damiano Altomare[1]

[1] Department of Pharmacy-Drug Sciences, University of Bari Aldo Moro, Via E. Orabona 4, 70125, Bari, Italy

[2] Univ. Grenoble Alpes, CEA, CNRS, Institute of Structural Biology, F-38044 Grenoble, France.

[3] Institute of Crystallography, National Research Council (CNR), Via G. Amendola 122/O, 70126 Bari, Italy

[4] Department of Food, Environmental and Nutritional Sciences (DeFENS), University of Milan, Via Celoria 2, 20133 Milano (Italy).

[5] Department of Biosciences, Biotechnologies and Biopharmaceutics, University of Bari Aldo Moro, Via E. Orabona 4, 70125, Bari, Italy

[6] Department of Neurobiology, Weizmann Institute of Science, 7610001 Rehovot, Israel.

Supporting Information

Materials and methods

1. Chemistry

Starting materials, reagents and analytical grade solvents were commercially available and purchased from Merck Sigma-Aldrich, Milan, Italy. All reactions were routinely monitored with thin layer chromatography (TLC) on aluminum sheets (Merck Kieselgel 60 F_{254}); spots were displayed through UV lamp. For reactions requiring anhydrous environment, glassware was preliminary dried by heating on flame burner and then by cooling under argon stream. Chromatographic separations were performed by means of gravitational chromatography, using 63-200 μm silica (Merck). Chiral HPLC analyses were performed using a Kromasil 5-AmyCoat column (4.6 mm i.d. × 250 mm, AkzoNobel), fitted to a Jasco PU-980 pump and a Jasco UV-975 detector (Jasco Europe, Cremella, Italy). Runs were carried out in 1/1 (v/v) hexane/iPrOH at a flow rate of 1 mL/min, monitoring the eluate at 220 nm. Preparative chiral HPLC was performed with a Kromasil 5-AmyCoat column (21.2 mm i.d. × 250 mm, Hichrom, Milan, Italy), fitted to a 1525 Extended Flow Binary HPLC pump and a Waters 2489 UV/Vis detector (both from Waters, Milan, Italy). Solvent was in 1/1 (v/v) hexane/iPrOH, at a flow rate of 15 mL/min, monitoring the eluate at 220 nm. ^{1}H-NMR spectra were recorded in the specified deuterated solvent at 500 MHz on an Agilent 500/54 Premium Shielded instrument (Agilent Technologies, Milan, Italy). Chemical shifts are expressed in δ (ppm) and coupling constants J in Hertz (Hz). The following abbreviations were used: s (singlet), t (triplet), qn (quintuplet), m (multiplet), br (broad signal); signals due to NH protons were located by deuterium exchange with D_2O. Melting points (MP) were determined by the capillary method on a Stuart Scientific SMP3 electrothermal apparatus (Bibby Scientific, Milan, Italy) and are uncorrected. Mass spectra were obtained with a dual electrospray interface (ESI) and a quadrupole time-of-flight mass spectrometer (Q-TOF, Agilent 6530 Series Accurate-Mass Quadrupole Time-of-Flight LC/MS, Agilent Technologies, Milan, Italy). Elemental analyses were performed on a Euro EA 3000 analyzer (Eurovector, Milan, Italy). Optical rotations were measured on a PerkinElmer 341 spectropolarimeter (PerkinElmer Ltd., Buckinghamshire, U.K.) at a concentration of 5 mg/mL in UV grade dichloromethane, with cell length of 1 dm.

Syntheses of compounds (±)-***cis*-1**, **2** and **3** have been already described.[1]

Scheme 1[a]

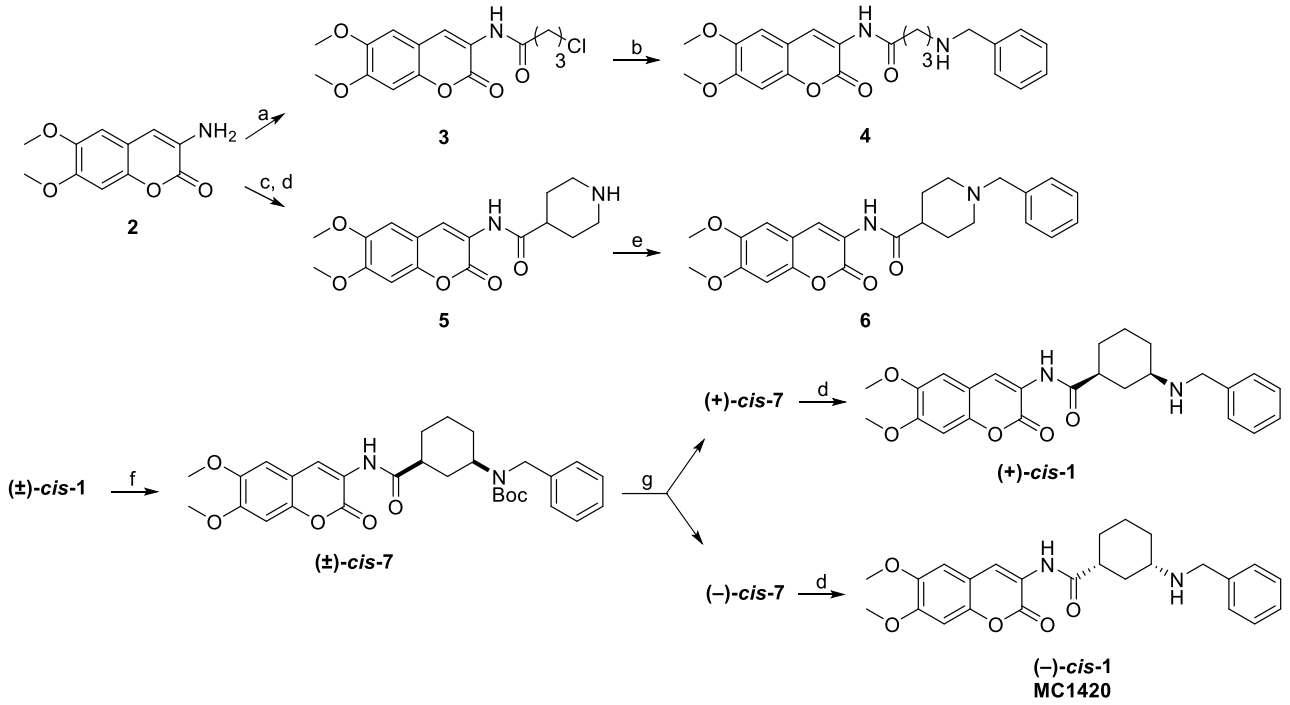

([a]) Reagents and conditions: (a), 4-chlorobutyryl chloride, THF, triethylamine, rt; (b), benzylamine, KI, acetone, rt; (c), N-Boc protected isonipecotic acid, HOBt, DIC, CH_2Cl_2, rt; (d), TFA, CH_2Cl_2, 0 °C. (e), benzyl bromide, K_2CO_3, acetone, rt; (f) Boc_2O, THF, rt; (g) semi-preparative chiral HPLC.

*1.1. Synthesis of **4-(benzylamino)-N-(6,7-dimethoxy-2H-2-oxochromen-3-yl)butyramide hydrochloride (4)***

121 mg (0.4 mmol) of **3**[1] (Scheme 1) dissolved in 3 mL of anhydrous acetone were added portionwise to a solution of 436 μL (0.4 mmol) of benzylamine in 3 mL of anhydrous acetone held at reflux. After 24 h the reaction was warmed to room temperature and the solvent was evaporated under vacuum. The crude oil was purified by column chromatography (eluent CH_2Cl_2/MeOH 9:1). The oil obtained by purification was treated with 1 mL of HCl 1.25N in ethanol yielding **4** as hydrochloride: yield 45%. MP 145-7 °C (dec); ^{1}H-NMR (DMSO-d_6) δ: 1.94 (qn, 2H, J = 8.0 Hz), 2.57 (t, 2H, J = 8.0 Hz); 2.97 (br, 2H); 3.80 (s, 3H); 3.84 (s, 3H); 4.58 (s, 2H); 6.98-7.52 (m, 7H); 8.57 (s, 1H); 8.89 (br, 2H, exch. D_2O); 9.10 (br, 1H, exch. D_2O). ESI-MS m/z: 395.4 $[M-H]^-$. Analytical calculated % for $C_{22}H_{24}N_2O_5 \cdot HCl$ C 61.04; H 5.82; N 6.47; found C 60.79; H 6.02; N 6.54.

*1.2. Synthesis of **N-(6,7-dimethoxy-2H-2-oxochromen-3-yl)piperidine-4-carboxamide (5)***

136 mg (0.54 mmol) of commercial N-Boc-piperidine-4-carboxylic acid and 90 mg (0.54 mmol) of 1-hydroxybenzotriazole were dissolved in 10 mL of anhydrous dichloromethane (DCM). After 5 min. the reaction was cooled to 0 °C trough an external ice bath and 92 µL (0.54 mmol) of N,N-diisopropylcarbodiimide were added dropwise. After 5 min 60 mg (0.27 mmol) of **2**[1] were added (Scheme 1) and the reaction was slowly warmed to room temperature and stirred for 36h. The mixture was filtered and the solvent was removed by rotatory evaporation. The resulting oil was concentrated to dryness yielding a brown solid. Purification by column chromatography (eluent ethyl acetate/n-hexane 2:1) afforded 1-Boc-N-(6,7-dimethoxy-2H-2-oxochromen-3-yl)piperidine-4-carboxamide as yellow solid: yield 98%. ESI-MS m/z: 455 $[M+Na]^+$, 431 $[M-H]^-$. 146 mg (0.27 mmol) of this intermediate were dissolved in 3 mL of a solution of TFA 50% in DCM at 0°C with stirring for 15 min. The reaction mixture was then warmed to room temperature and stirred for 5h. The resulting acid solution was neutralized with $NaHCO_3$, the inorganic precipitate filtered off and washed with DCM. The solution was extracted with DCM (3×20 mL) and the organic layers were collected and dried over anhydrous Na_2SO_4. The solvent was removed by rotatory evaporation yielding an orange solid: yield 84%. ^{1}H-NMR (acetone-d_6) δ: 1.62-1.76 (m, 2H); 1.92-1.96 (m, 2H); 2.74-2.79 (m, 2H); 2.96-3.26 (m, 2H); 3.86-3.69 (m, 1H); 3.90 (s, 3H); 3.93 (s, 3H); 5.03 (br, 1H, exch. D_2O); 6.98 (s, 1H); 7.22 (s, 1H); 8.58 (br, 1H, exch. D_2O); 8.65 (s, 1H). ESI-MS m/z : 355.4 $[C_{17}H_{20}N_2O_5 + Na]^+$.

1.3. Synthesis of ***1-benzyl-N-(6,7-dimethoxy-2H-2-oxochromen-3-yl)piperidine-4-carboxamide (6)***

67 mg (0.15 mmol) of **5** (Scheme 1) and 10 mg (0.7 mmol) of K_2CO_3 were suspended in 2 mL of anhydrous acetone. 0.018 mL (0.15 mmol) of benzyl bromide were added and the mixture stirred for 24 h at room temperature. The salt was filtered and washed with acetone and THF and the solvent was concentrated under vacuum. A brown solid was obtained and purified by column chromatography (eluent DCM/MeOH 95:5) yielding a yellow solid: yield 65%. MP 151-4 °C (dec). ^{1}H-NMR ($CDCl_3$) δ: 2.11-2.18 (m, 2H); 2.68-2.78 (m, 4H); 3.23-3.38 (m, 2H); 3.79-3.83 (m, 1H); 3.91 (s, 3H); 3.93 (s, 2H); 3.94 (s, 3H); 6.83-6.92 (m, 3H); 7.44-7.49 (m, 4H); 7.71 (br, 1H, exch. D_2O); 8.58 (s, 1H). ESI-MS m/z: 445.3 $[M+Na]^+$, 421.3 $[M-H]^-$. Analytical calculated % for $C_{24}H_{26}N_2O_5$ C 68.23; H 6.20; N 6.63; found C 68.44; H 6.41; N 6.36.

*2. Chromatographic resolution of (±)-cis-**1**.*

125 mg of chromatographically pure (±)-*cis*-**1** (0.28 mmol) were dissolved in 5 mL of anhydrous THF; 87 mg of di-*t*-butyldicarbonate (0.40 mmol) were added and the solution stirred at room temperature for 6 h (Scheme 1). The solvent was evaporated to dryness and the crude residue purified on column chromatography (eluent ethyl acetate/*n*-hexane 1:1), giving (±)-***cis*-7** in quantitative yield.

The separation of the two enantiomers (+)-*cis*-**7** and (−)-*cis*-**7** was carried out with a Kromasil 5-AmyCoat (21.2 × 250 mm) chiral stationary phase with isopropanol/n-hexane 1:1 v/v as the eluent (flow rate 15 mL/min; λ = 220 nm). (+)-**7**, t_R = 9.8 min; $[\alpha]_D^{25}$= + 34 deg·mL·dm^{-1}·g^{-1} (5 mg/mL; DCM). (−)-**7**, t_R = 14.5 min; $[\alpha]_D^{25}$= – 34 deg·mL·dm^{-1}·g^{-1} (5 mg/mL; DCM).

After separation, compounds (+)-**7** and (−)-**7** (48 mg each, 0.09 mmol) were deprotected by dissolving them in 3 mL of trifluoroacetic acid 10% in DCM at 0 °C. After the same workup described above for **5**, pure final compounds were obtained in quantitative yield. ^{1}H-NMR and ESI-MS spectra were fully consistent with those previously described for (±)-***cis*-1**.[1] Both free bases were crystallized as hydrochloride from a solution of HCl 1.25N in ethanol: MP 193-5 °C (dec). Analytical calculated % for $C_{25}H_{28}N_2O_5$·HCl·1.5 H_2O C 60.06; H 6.45; N 5.60; found (+)-*cis*-**1** C 60.04; H 6.19; N 5.51; (−)-*cis*-**1** C 59.77; H 6.26; N 5.61. (+)-*cis*-**1**, $[\alpha]_D^{25}$ = + 50 deg·mL·dm^{-1}·g^{-1} (5 mg/mL; DCM); (−)-*cis*-**1**, $[\alpha]_D^{25}$ = − 50 deg·mL·dm^{-1}·g^{-1} (5 mg/mL; DCM).

3. Enzyme inhibition assays

Inhibition of human acetylcholinesterase (*h*AChE) in phosphate buffer pH 8.0 was assessed by means of the classical Ellman's assay,[2] implemented on a 96-well plate procedure.[3] Butyrylcholinesterase (*h*BChE) was also assayed to assess AChE/BChE selectivity. Inhibition kinetics of (±)-*cis*-**1** and its enantiomers were determined for *h*AChE (Table 1). Acetyl- or butyrylthiocholine iodide were used as substrate and 5,5'-dithiobis(2-nitrobenzoic acid) (DTNB) as the chromophoric reagent. All enzymes and reagents were purchased from Sigma Aldrich Italy. Solutions of tested compounds were prepared starting from 10 mM stock solutions in DMSO, that were diluted with aqueous assay medium to a final content of organic solvent always lower than 1%. ChE-catalyzed hydrolysis was followed by measuring the increase of absorbance at 412 nm every 30 sec for 5 min at 25 °C using a 96-well microplate reader Infinite M1000 Pro (Tecan, Milan, Italy). The concentration of compound which yielded 50% inhibition of the ChE activity (IC_{50}) was calculated by non-linear regression of the response–log(concentration) curve, using GraphPad Prism (GraphPad Prism version 5.00 for Windows, GraphPad Software, San Diego, CA,

USA). Kinetic studies were performed in the same incubation conditions, using six concentrations of substrate (from 0.033 to 0.200 mM) and four concentrations of inhibitor in a range comprising the IC_{50} value. Inhibition constants and kinetic parameters were calculated within the "Enzyme kinetics" module of Prism.

4. MTT assays.

Cytotoxicity of compound (±)-*cis*-**1** was assayed on HepG2 human liver cancer cell line and on Madin-Darby canine kidney cells (MDCK-MDR1), by a MTT-based assay previously described.[4] Briefly, viable cells were seeded in a sterile 96-well plate Cell Culture Cluster (Corning, NY, USA) and incubated with different concentrations of tested compounds for 2 h (on HepG2 cells), 24 and 72 h (on MDCK-MDR1 cells) at 37 °C in 5% CO_2. At the end of incubation, the culture medium was replaced by a solution of MTT 0.5 mg/mL in PBS. After 4 h incubation at 37 °C in 5% CO_2 the supernatants were aspirated and 100 μL of DMSO were added to each well. The absorbance at 570 nm was measured using a plate reader Victor V3 (Perkin-Elmer, Milan, Italy). Results are expressed as the percentage of MTT reduction respect to control cells. All experiments were carried out in sextuplicate and were repeated twice.

5. Permeability assays.

Blood-brain barrier permeability was estimated with a cellular model using transfected Madin-Darby canine kidney cells (MDCK-MDR1) expressing P-glycoprotein (P-gp),[5] as previously described.[6] Briefly, MDCK-MDR1 cells were seeded at a concentration of 1×10^5 cells per well on the apical side of Transwell inserts, in DMEM medium supplemented with 10% heat-inactivated fetal bovine serum (FBS), 100 U/mL penicillin, 100 μg/mL streptomycin and 2 mM L-glutamine (EuroClone, Milan, Italy). Cells were maintained at 37 °C, 5% CO_2, and saturated humidity. Monolayer formation (approximately 8 days after seeding) was monitored by microscopy, and the TEER (Trans Epithelial Electrical Resistance) was measured every day using an EVOM electrode epithelial volt-ohm meter (World Precision Instruments, Friedberg, Germany). Formation of tight junctions was assessed by measuring the flux of the transcellular standard diazepam (75 μM) and of paracellular standard fluorescein isothiocyanate-dextran (FD4, Sigma) (200 μg/mL) from the apical to the basolateral compartment. These probes were quantified with a PE double-beam UV-visible spectrophotometer Lambda Bio 20 (PerkinElmer, Milan, Italy) and a Victor3 fluorimeter (Wallac Victor3, 1420 Multilabel Counter, Perkin-Elmer) at excitation and emission wavelengths of 485 and

535 nm, respectively. The apparent permeabilities (P_{app}), in units of cm/sec, in both directions, were calculated using the following equation S1:

$$P_{app}=(V_a/area\times time)\times([Drug]acceptor/[Drug]initial) \qquad (eq.\ S1)$$

where "V_a" is the volume in the acceptor well, "area" is the surface area of the membrane, "time" is the total transport time, "[Drug] acceptor" is the concentration of the drug measured by UV-spectroscopy and "[Drug] initial" is the initial drug concentration in the Apical (AP) or Basolateral (BL) chamber.

To assess the P_{app} AP or BL, across the BBB, *(±)-cis*-**1** was added to the apical or to basolateral compartment of the Transwell model in 0.5 mL or 1.5 mL of PBS (EuroClone, Milan, Italy), respectively, at a concentration of 75 µM. The receiving compartments contained 1.5 mL or 0.5 mL of PBS, respectively. After 2 h of incubation, the medium in the apical and basolateral compartments were collected separately. *(±)-cis*-**1** was quantified through UV-visible spectroscopy using the UV-visible spectrophotometer Lambda Bio 20 equipped with 10 mm path-length-matched quartz cells. P_{app} AP (cm/sec) and P_{app} BL (cm/sec) were calculated as described above. The efflux ratio (ER) was calculated using the following equation S2:

$$ER=(P_{app},\ BL\text{-}AP)/(P_{app},\ AP\text{-}BL) \qquad (eq.\ S2)$$

P_{app}, BL-AP: apparent permeability of basal-to-apical transport; P_{app}, AP-BL: apparent permeability of apical-to-basal transport. An efflux ratio greater than 2 indicates that a test compound is likely to be a substrate for P-gp transport.

Table S1. MDCK-MDR1 cell MTT assay.[a]

Entry	% cell viability at [drug]= 100 µM		IC_{50} (µM)
	24 h	72 h	72 h
(±)-*cis*-**1**	60 ± 2	37 ± 2	30.2 ± 1.6

([a]) Values are mean ± SEM of three independent experiments.

6. Hydration calculations.

Hydration calculations were performed on **MC1420** independently from crystallographic data, to identify protein-ligand interactions mediated by water molecules, by using WET,[7] a python script included in the AUTODOCK v. 4.2 docking suite.[8] The hydration procedure consists of the following steps: i) H-bond donors and acceptors in the ligand are recognized; ii) the ligand is

saturated with water molecules along H-bond vectors from the heavy atoms; iii) water molecules positions are checked against experimental occurrences.[9-12] The procedure provides 12 water molecules, two of them that are involved in H-bonds with oxygen of the amidic group of the ligand and N of the amidic group of Phe288. Such interactions are similar to that of the experimentally obtained W1 water molecule. Figure S1 shows that water molecules obtained by WET (cyan spheres) are close to W1 water molecule (red sphere).

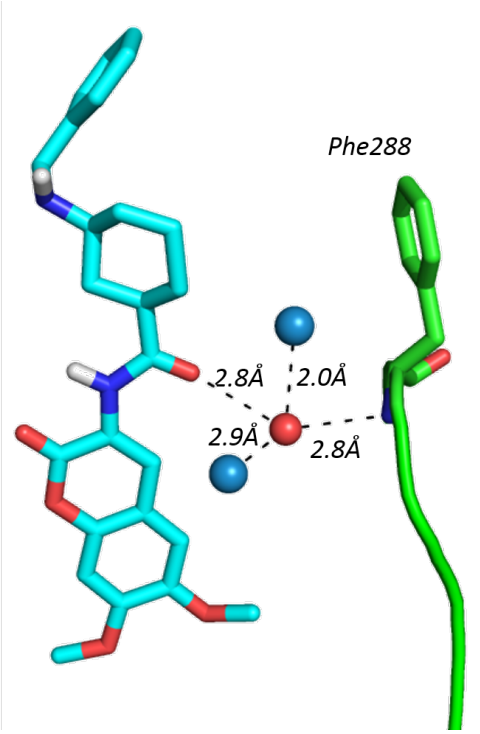

Figure S1. Water-mediated interaction of **MC1420** with *Tc*AChE. The ligand (cyan) and Phe288 (green) are both shown as sticks. Water molecules placed according to the experimental electron density map (W1, red sphere) and obtained by the hydration procedure (cyan spheres) are shown. Bonds between water molecules, and H-bond interactions mediated by waters, are shown by dashed lines.

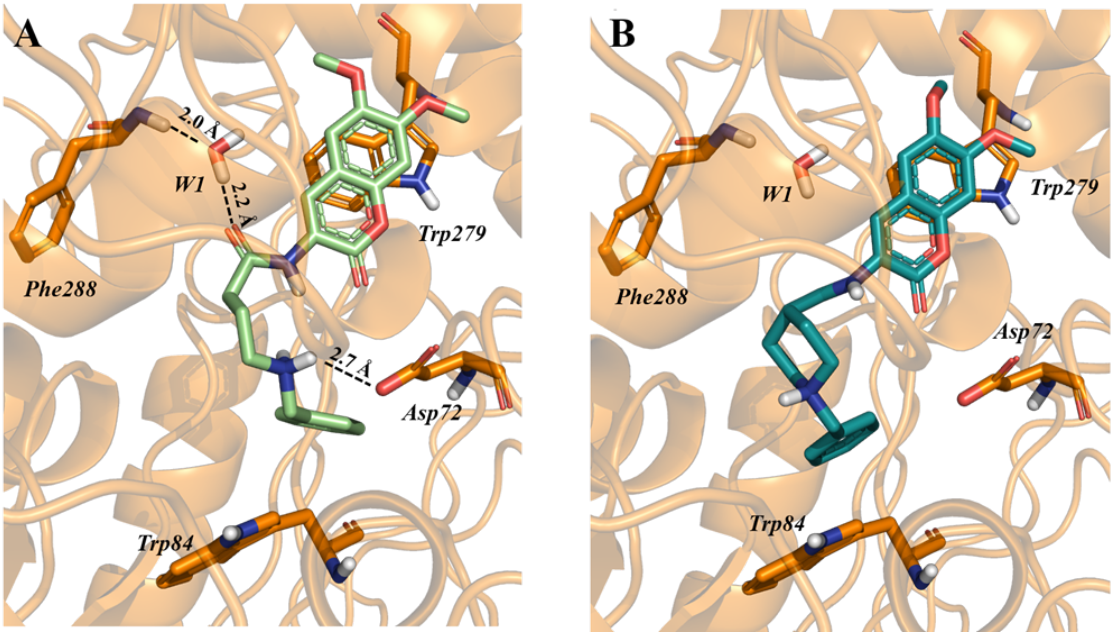

Figure S2. Top-scored docking poses of **4** (A) and **6** (B) within the binding site of *Tc*AChE. The ligand itself, relevant amino acid residues, and the water molecule W1 responsible for water-mediated interaction with Phe288, are all rendered as sticks, while protein is represented as cartoon. H-bonds are depicted by dotted lines.

Table S2. Data collection and refinement statistics.

	MC1420
PDB ID	6TT0
Wavelength (Å)	1.074
Resolution range	39.48 - 2.8 (2.9 - 2.8)
Space group	P 31 2 1
Unit cell	111.42 111.42 137.37 90 90 120
Total reflections	44657 (4385)
Unique reflections	24409 (2405)
Multiplicity	1.8 (1.8)
Completeness (%)	98.06 (98.81)
Mean I/sigma(I)	10.50 (1.57)

Wilson B-factor	69.73
R-merge	0.04067 (0.3768)
R-meas	0.05751 (0.5328)
R-pim	0.04067 (0.3768)
CC1/2	0.998 (0.872)
CC*	1 (0.965)
Reflections used in refinement	24321 (2407)
Reflections used for R-free	1189 (124)
R-work	0.1896 (0.3374)
R-free	0.2370 (0.3933)
CC(work)	0.958 (0.862)
CC(free)	0.957 (0.705)
Number of non-hydrogen atoms	4392
Macromolecules	4244
Ligands	60
Solvent	88
Protein residues	532
RMS(bonds)	0.012
RMS(angles)	1.08
Ramachandran favored (%)	93.58
Ramachandran allowed (%)	6.04
Ramachandran outliers (%)	0.38
Rotamer outliers (%)	5.38
Clashscore	9.02
Average B-factor	69.92
Macromolecules	69.82
Ligands	77.83
Solvent	69.26

*Statistics for the highest-resolution shell are shown in parentheses.

References

1. Catto, M.; Pisani, L.; Leonetti, F.; Nicolotti, O.; Pesce, P.; Stefanachi, A.; Cellamare, S.; Carotti, A. Design, Synthesis and Biological Evaluation of Coumarin Alkylamines as Potent and Selective Dual Binding Site Inhibitors of Acetylcholinesterase. *Bioorg. Med. Chem.* **2013**, *21*, 146-152.

2. Ellman, G. L.; Courtney, K. D.; Andres, V., Jr.; Feartherstone, R. M. A New and Rapid Colorimetric Determination of Acetylcholinesterase Activity. *Biochem. Pharmacol*. **1961**, *7*, 88-95.

3. Pisani, L.; Catto, M.; De Palma, A.; Farina, R.; Cellamare, S.; Altomare, C. D. Discovery of Potent Dual Binding Site Acetylcholinesterase Inhibitors via Homo- and Heterodimerization of Coumarin-Based Moieties. *ChemMedChem* **2017**, *12*, 1349-1358.

4. Berridge, M. V.; Tan, A. S. Characterization of the Cellular Reduction of 3-(4,5-Dimethylthiazol-2-yl)-2,5-diphenyltetrazolium Bromide (MTT): Subcellular Localization, Substrate Dependence, and Involvement of Mitochondrial Electron Transport in MTT Reduction. *Arch. Biochem. Biophys.* **1993**, *303*, 474-482.

5. Franchini, S.; Manasieva, L.I.; Sorbi, C.; Battisti, U. M.; Fossa, P.; Cichero, E.; Denora, N.; Iacobazzi, R. M.; Cilia, A.; Pirona, L.; Ronsisvalle, S.; Aricò, G.; Brasili, L. Synthesis, Biological Evaluation and Molecular Modeling of 1-Oxa-4-thiaspiro- and 1,4-Dithiaspiro[4.5]decane Derivatives as Potent and Selective 5-HT_{1A} Receptor Agonists. *Eur. J. Med. Chem.* **2017**, *125*, 435-452.

6. Pisani, L.; Farina, R.; Soto-Otero, R.; Denora, N.; Mangiatordi, G. F.; Nicolotti, O.; Mendez-Alvarez, E.; Altomare, C. D.; Catto, M.; Carotti, A. Searching for Multitargeting Neurotherapeutics against Alzheimer's: Discovery of Potent AChE−MAO B Inhibitors through the Decoration of 2H-Chromen-2-one Structural Motif. *Molecules* **2016**, *21*, 362.

7. Forli, S.; Olson, A. J. A Force Field with Discrete Displaceable Waters and Desolvation Entropy for Hydrated Ligand Docking. *J. Med. Chem*. **2012**, *55*, 623-638.

8. Morris, G. M.; Huey, R.; Lindstrom, W.; Sanner, M. F.; Belew, R. K.; Goodsell, D. S.; Olson, A. J. Autodock4 and AutoDockTools4: Automated Docking with Selective Receptor Flexibility. *J. Comput. Chem*. **2009**, *16*, 2785-2791.

9. Taylor, R.; Kennard, O.; Versichel, W. Geometry of the Imino-Carbonyl (N-H...O:C) Hydrogen Bond. 1. Lone-Pair Directionality. *J. Am. Chem. Soc*. **1983**, *105*, 5761-5766.

10. Wiberg, K.; Marquez, M.; Castejon, H. Lone Pairs in Carbonyl-Compounds and Ethers. *J. Org. Chem*. **1994**, *59*, 6817-6822.

11. Lommerse, J. P. M.; Price, S. L.; Taylor, R. Hydrogen Bonding of Carbonyl, Ether, and Ester Oxygen Atoms with Alkanol Hydroxyl Groups. *J. Comput. Chem*. **1997**, *18*, 757-774.

12. Nobeli, I.; Price, S. L.; Lommerse, J. P. M.; Taylor, R. Hydrogen Bonding Properties of Oxygen and Nitrogen Acceptors in Aromatic Heterocycles. *J. Comput. Chem*. **1997**, *18*, 2060-2074.